ACS OMEGA

http://pubs.acs.org/journal/acsodf

Article

Angular-Shaped Boron Nitride Nanosheets with a High Aspect Ratio to Improve the Out-of-Plane Thermal Conductivity of Polyimide Composite Films

Song Zuo, Yu Lan, Jinpeng Luo, Fei Zhou, Lexiang Xu, Shaoxiong Xie, Xiuqin Wei, Lang Zhou, Lei Ma, Xiaomin Li,* and Chuanqiang Yin*

Cite This: *ACS Omega* 2022, 7, 43273−43282

Read Online

ACCESS | Metrics & More | Article Recommendations

ABSTRACT: Polyimide/boron nitride nanosheet (PI/BNNS) composite films have potential applications in the field of electrical devices due to the superior thermal conductivity and outstanding insulating properties of the boron nitride nanosheet. In this study, the boron nitride nanosheet (BNNS-t) was prepared by the template method using sodium chloride as the template, and B_2O_3 and flowing ammonia as the boron and nitrogen sources, respectively. Then, the PI/BNNS-t composite films were investigated with different loading of BNNS-t as thermally conductive fillers. The results show that BNNS-t has a high aspect ratio and a uniform lateral dimension, with a large dimension and a thin thickness, and there are a few nanosheets with angular shapes in the as-obtained BNNS-t. The synergistic effect of the above characteristics for BNNS-t is beneficial to constructing the three-dimensional heat conduction network of the PI/BNNS-t composite films, which can significantly improve the out-of-plane thermal conduction properties. And then, the out-of-plane thermal conductivity of the PI/BNNS-t composite film achieves 0.67 W m^{-1} K^{-1} at 40% loading, which is nearly 3.5 times that of the PI film.

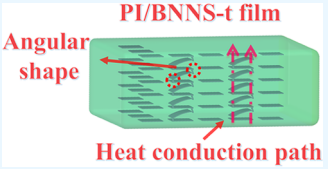

1. INTRODUCTION

With the development of miniaturized electronic gadgets and high-power electronics such as light-emitting diodes (LED),[1−3] solar cells,[4−6] and chips,[7−9] higher requirements are put forward for heat dissipation materials. Polyimide (PI) films have attracted great interest for the potential application of heat dissipation materials due to their outstanding mechanical characteristics, chemical resistance, lightweight, and ease of fabrication. However, PI films cannot be directly used as heat dissipation materials due to their poor intrinsic thermal conductivity (0.2 W m^{-1} K^{-1} or so).[10,11] Therefore, to satisfy application requirements in the field of thermal management, inorganic materials are usually added to the PI matrix to enhance the thermal properties of the PI composite films. Among various inorganic fillers, boron nitride nanosheets (BNNS) are an ideal candidate for the fillers of PI composite films because of their excellent thermal conductivities (300−2000 W m^{-1} K^{-1}) and insulating properties (5.0−6.0 eV band gap).[12−14]

There are several methods to prepare BNNS, such as the ball milling method, the sonication method, and the chemical vapor deposition method. For instance, from the early scotch tape approach[15] to the more mature ball milling process,[16−20] the large-scale and inexpensive synthesis production of BNNS has been realized using the mechanical cleavage method. However, the lateral size and homogeneity of BNNS can be significantly reduced due to the high shear and compressive forces generated during the ball milling preparation. Besides, the method based on a microfluidization technique[21,22] has recently been shown to generate shear rates sufficient to cause exfoliation of the hexagonal boron nitride (h-BN). The advantage of the above method is that the high-aspect-ratio BNNS with considerable yields can be prepared without particle size separation. However, the uneven particle size distribution of the final product and the time wasted caused by the excessive number of loops limit its development. In addition, the sonication process[23−27] is utilized to achieve the stripping of h-BN due to the cavitation effect of ultrasonic waves and the strong interaction between the solvent and the surface of h-BN. Still, the high cost of organic solvent and the damage to the lateral size of BNNS inhibit its application. Additionally, the chemical vapor deposition method[28−30] can deposit the high-quality BNNS on the surfaces of substrates using two or more precursors. However, the application of this method is not ideal due to the complex operation and low yield. Moreover, the high-temperature chemical reaction method[31,32] is often utilized to produce commercial h-BN. However, when producing BNNS, it is limited by a low yield or

Received: September 17, 2022
Accepted: November 3, 2022
Published: November 15, 2022

https://doi.org/10.1021/acsomega.2c06013
ACS Omega 2022, 7, 43273−43282

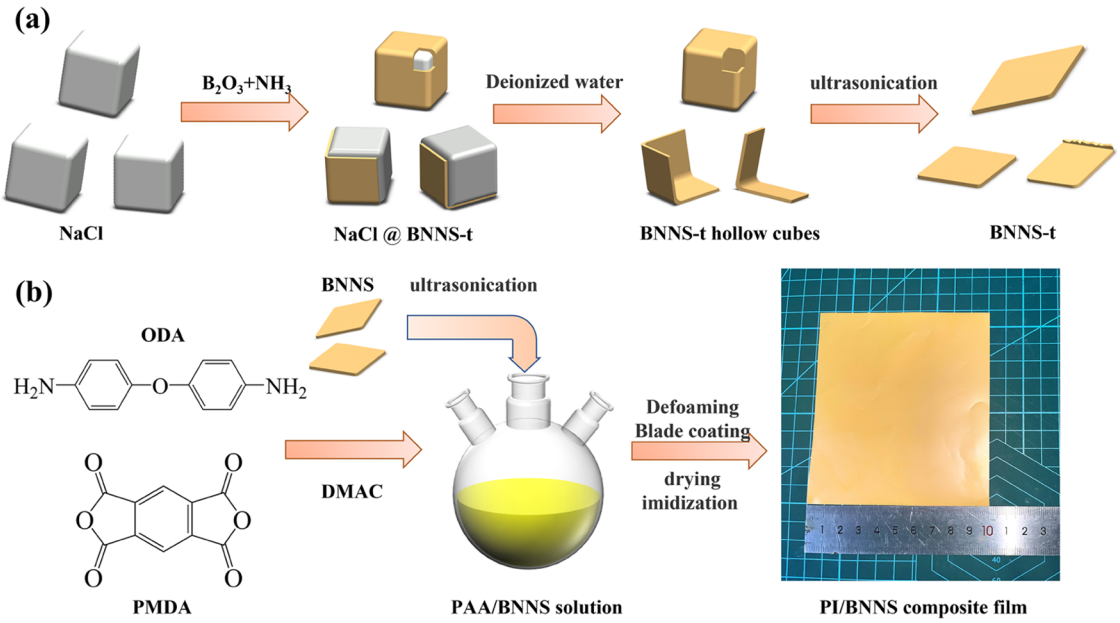

Figure 1. Schematic illustration for the preparation of (a) BNNS-t and (b) PI/BNNS composite films.

the high cost of raw materials. As a result, the two-dimensional nanosheets are obtained using the above-mentioned methods for preparing BNNS, which mainly have a positive effect on the in-plane thermal conductivity of the composite material, and the improvement of the out-of-plane thermal conductivity is relatively limited.

To improve the out-of-plane thermal conductivity of the composite material and better satisfy the heat dissipation requirements of particular electronic components, it is primarily realized by the method of inorganic thermal conductive particle bridging. That is, zero-dimensional (0D) and one-dimensional (1D) thermally conductive fillers are compounded with two-dimensional (2D) BNNS to form an uninterrupted heterogeneous thermally conductive structure such as a point surface or line surface in the composite matrix. The improvement of the out-of-plane thermal conductivity of the composite with heterogeneous thermally conductive fillers is limited due to its relatively low intrinsic thermal conductivity and poor bridge-contact sites. In addition, the construction of three-dimensional (3D) network skeleton structures (such as the ice template method,[33] 3D skeleton method,[34] and 3D printing method)[35] is common in polymer thermally conductive composites. However, this method is difficult to implement in PI composite films with a thickness of less than 100 μm.

The NaCl template is an excellent method to prepare BNNS.[36] In this study, an angular-shaped boron nitride nanosheet with a high aspect ratio was proposed and verified to improve the out-of-plane thermal conductivity of the composite as a network structure unit with a uniform thermal conductivity. The boron nitride nanosheets (BNNS-t) with a high aspect ratio and uniform lateral dimension were prepared and characterized by the NaCl template method, which is applied to PI/BNNS-t composite films to improve the out-of-plane thermal conductivity of composites. The angular-shaped structure appearing in the part of BNNS-t implements the homogeneous point-plane and line-plane bridging of BNNS-t in the PI matrix. In addition, the high aspect ratio of BNNS-t enables the composite to obtain a higher thermal conductivity at a lower load. Therefore, the synergistic effect of the above characteristics for BNNS-t is beneficial to constructing the 3D heat conduction network of the PI/BNNS-t composite films, which can significantly improve the out-of-plane thermal conduction properties.

2. EXPERIMENTAL SECTION

2.1. Materials. Sodium chloride (NaCl, AR), anhydrous ethanol (C_2H_6O, 99.7%), and sodium hydroxide (NaOH, AR) were obtained from Sinopharm Chemical Reagent Co., Ltd. Shanghai Aladdin Biochemical Technology Co., Ltd. provided boron oxide (B_2O_3, 99.9%) and h-BN powder. *N*,*N*-Dimethylacetamide (DMAc, AR) was supplied by Sinopharm Chemical Reagent Co., Ltd. Pyromellitic dianhydride (PMDA, 99.5%) was obtained from Zhiyu Granule New Material Co., Ltd. 4,4′-Oxydianiline (ODA, 99.5%) was provided by Wanda Chemical Co., Ltd. All materials were utilized as supplied with no additional refinement.

2.2. Preparation of BNNS. As shown in Figure 1a, the preparation process of BNNS-t is exhibited in detail. First, micron-sized NaCl crystals were obtained by adding anhydrous ethanol to a saturated sodium chloride solution. Second, the recrystallized NaCl and B_2O_3 were adequately mixed at a mass ratio of 4:1 to obtain the powder mixture, and the powder mixture was placed in an alumina crucible. Third, the alumina crucible was put into the heating area of the tube furnace, heated to 500 °C at 10 °C/min under flowing argon (100 sccm), and maintained for 10 min. Then, the flowing argon was switched to the flowing ammonia (150 sccm), and the temperature was raised to 700 °C at 10 °C/min (the melting point of NaCl is 801 °C) and maintained for 30 min. After that, the temperature was increased to 1100 °C at 10 °C/min, maintained for 10 min, and then decreased to room temperature under the flowing argon (60 sccm). Lastly, the obtained unprocessed powder was cleaned with deionized water, sonicated (60 W, 1 h) in a mixed solution of water and trace alcohol, vacuum filtered, and dried at 90 °C for 12 h to obtain BNNS-t.

https://doi.org/10.1021/acsomega.2c06013
ACS Omega 2022, 7, 43273−43282

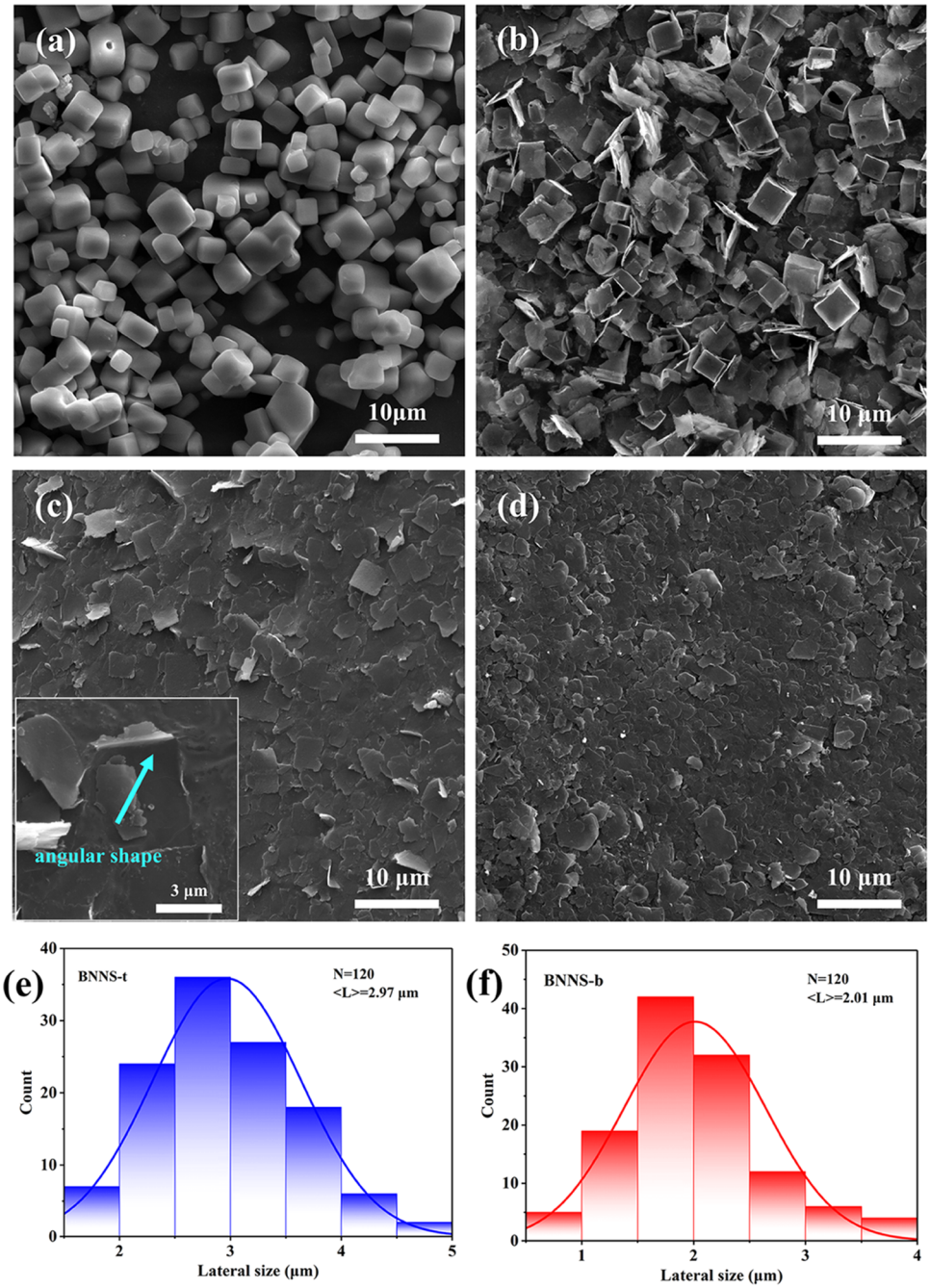

Figure 2. SEM images of (a) the NaCl template after recrystallization, (b) BNNS-t after NaCl cube template removal, (c) BNNS-t, and (d) BNNS-b; the lateral size distribution of (e) BNNS-t and (f) BNNS-b.

As a reference, another BNNS was obtained by the ball milling process. In a nutshell, after combining h-BN and an aqueous sodium hydroxide solution, the mixture was put into a jar and milled for 8 h at 400 rpm by a planetary ball mill. The finished product was then cleaned with deionized water, centrifugal separation treatment, and dried to get BNNS. For convenience, the as-obtained product by the ball milling process was abbreviated as BNNS-b.

2.3. Preparation of PI/BNNS Composite Films. As shown in Figure 1b, the preparation process of PI/BNNS composite films is briefly presented. First, ODA and PMDA with the same mole fraction were mixed at room temperature with DMAc as the solvent and stirred in a 250 mL three-necked flask. Then, the polyimide acid (PAA) solution was obtained by polycondensation. After ultrasonic treatment (60 W, 2 h) of BNNS with the different mass fractions, they were separately added to the PAA solution and uniformly mixed for 10 h to obtain the PAA/BNNS solution. After that, the PAA/BNNS solution was vacuum defoamed, blade coated, and dried at 100 °C for 1 h. Lastly, the PAA/BNNS composite films were transferred to a muffle furnace for thermal amination treatment. Specifically, the samples were heated to 150 °C for 1 h, then heated to 250 °C for 1 h, and finally heated to 350 °C for 1 h to obtain the PI/BNNS composite films. Meanwhile, the PI/BNNS composite films with different loading of BNNS-t or BNNS-b (10, 20, 30, and 40% relative to the mass fraction of PI) were labeled as 10-BNNS-t, 20-PI/

https://doi.org/10.1021/acsomega.2c06013
ACS Omega 2022, 7, 43273−43282

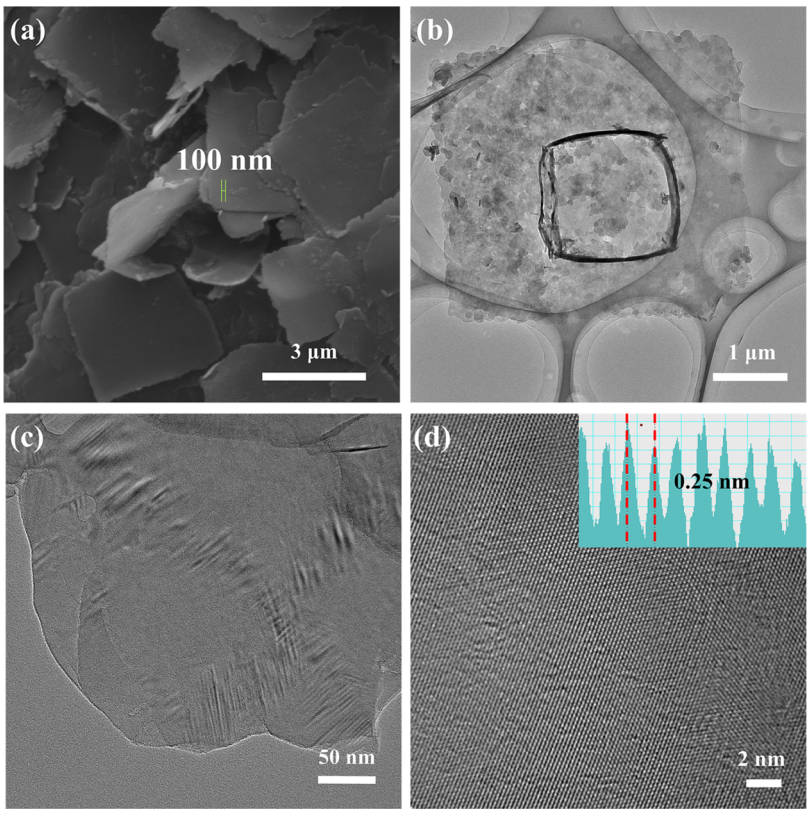

Figure 3. (a) SEM image of BNNS-t, (b, c) TEM image of BNNS-t, (d) HRTEM image showing the lattice fringes of the (100) plane with 0.25 nm.

BNNS-t, 30-PI/BNNS-t, 40-PI/BNNS-t, 10-PI/BNNS-b, 20-PI/BNNS-b, 30-PI/BNNS-b, and 40-PI/BNNS-b, respectively.

2.4. Characterization. The microstructure of the samples was observed under a scanning electron microscope (SEM, Phenom LE) under the conditions of secondary electron and an operating voltage of 15 kV. The structure of the BNNS-t powder was further observed under a field emission transmission electron microscope (TEM, JEM-2100, Jeol, Japan). The crystal structure and chemical composition of samples were tested by the Reflex Raman System (alpha300R, WITec, Germany), Fourier transform infrared spectrometer (FT-IR, iS50, Thermo Fisher Scientific, Inc), X-ray diffractometer (XRD, D8 Discover, Bruker, Germany), and X-ray photoelectron spectrometer (XPS, ESCALAB25OXi, Thermo Fisher Scientific). The thermal diffusivity (α) of the PI/BNNS composite films was measured by the laser flash analyzer (LFA 447, Netzsch, Germany), the density (ρ) was obtained by the density balance, and the specific heat capacity (C_p) was measured by the differential scanning calorimeter (DSC200F3, Netzsch, Germany). The thermal conductivity (κ) of the PI/BNNS composite films is calculated by the equation

$$\kappa = \alpha \times \rho \times C_p \quad (1)$$

The heat source was provided by an LED light sticker (3 W), and the infrared images and the temperature change curve of the composite films were recorded by the infrared imager (IRay AT61P8DSHX, IRay, China).

3. RESULTS AND DISCUSSION

3.1. Characterization of BNNS. As shown in Figure 2, to clarify the synthesis steps of BNNS-t, the key SEM images of products in each stage and the SEM images of reference BNNS-b are clearly exhibited. Figure 2a shows that the particle sizes of the recrystallized NaCl are homogeneous and at about 3 μm. The requirements of the NaCl template can be satisfied with a low content owing to the substantial specific surface area of the as-obtained micron NaCl, and the uniform particle size of the recrystallized NaCl ensures that the as-prepared BNNS-t has a homogeneous transverse size, which can be seen from Figure 2b. However, the structure of the BNNS-t in the image indicates that this method is unstable, with some examples having an empty shell structure and others having a two-dimensional (2D) sheet structure. The uniform shape of the as-obtained BNNS-t can be attributed to the fact that the B_2O_3 completely melts at 500 °C and forms a liquid coating on the surface of the NaCl cube template before the introduction of ammonia gas. The inconsistent reactivity of the liquid B_2O_3 on the six surfaces of the NaCl cube template grain can be ascribed to the limited gas flow of ammonia, resulting in a poor connection between BNNS-t obtained on one surface and that on the other surface. During ultrasonication, the cubic shell structure is precarious, and it is easy to break along the edges to form the desired 2D BNNS-t. As shown in Figure 2c,d, the as-obtained BNNS-t is a homogeneous square sheet, while BNNS-b is a sheet with varied forms. To precisely quantify the lateral dimension of the BNNS, as displayed in Figure 2e,f, the distributions of the lateral dimension are tallied from 120 sheets. The results show that the mean transverse dimensions of BNNS-t and BNNS-b are 2.97 μm and 2.01 μm, respectively, which indicates that a uniform and larger diameter can be obtained using the NaCl template method. Meanwhile, since BNNS-t is generated by subjecting the BNNS-t cubic shell to ultrasonication, some angular-shaped nanosheets will

https://doi.org/10.1021/acsomega.2c06013
ACS Omega 2022, 7, 43273−43282

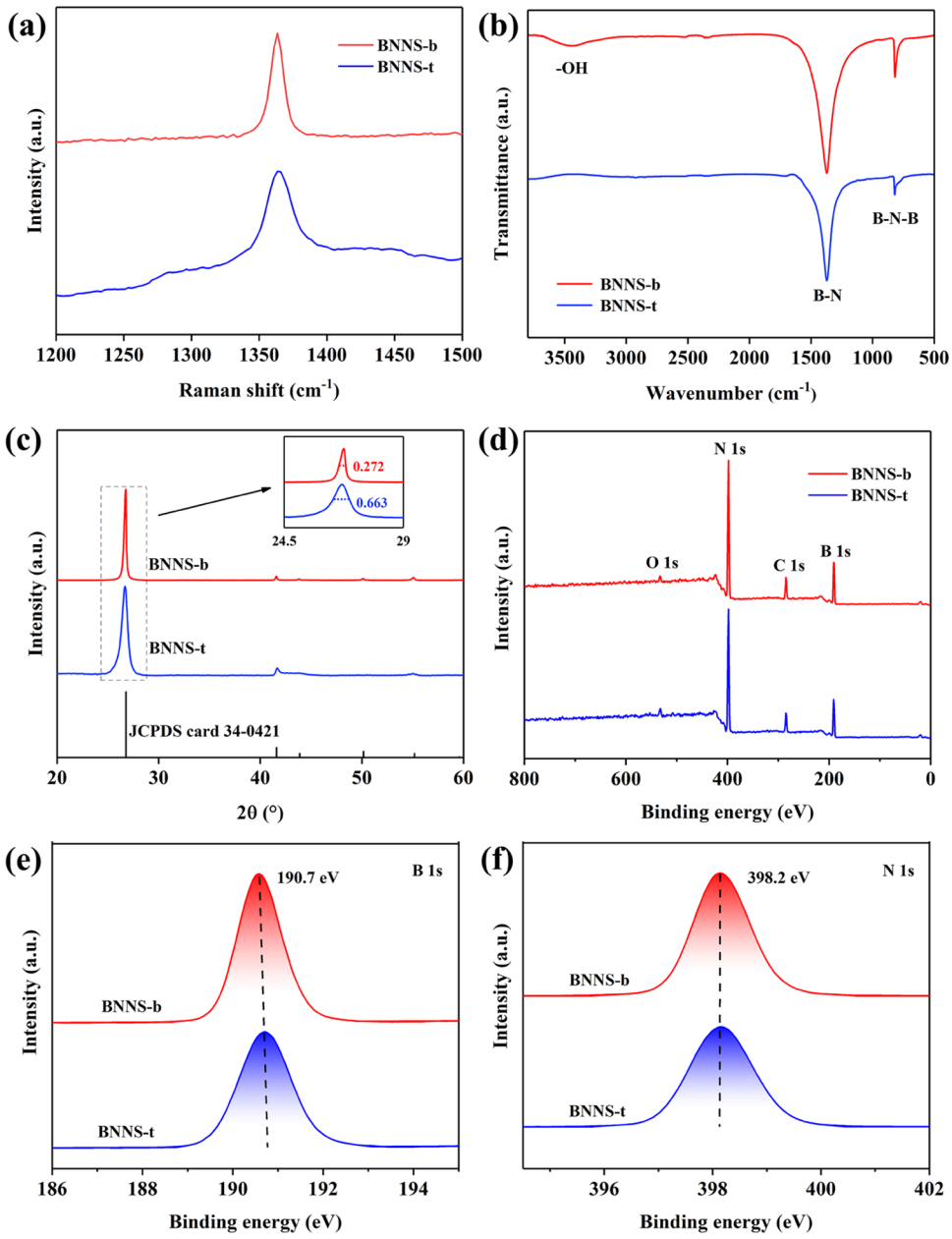

Figure 4. (a) Raman, (b) FT-IR, (c) XRD, and (d–f) XPS spectra of BNNS-t and BNNS-b.

remain inevitably on the edge of a few BNNS-t, as displayed in the inset of Figure 2c, which is advantageous for the out-of-plane thermal conductivity. In addition, a total yield can be achieved with a value of 77% by synthesizing 2.2 g of BNNS-t from 4 g of B_2O_3 through all of the synthetic stages. Thus, the as-obtained BNNS-t has a high application value due to its homogeneous transverse size, large particle size, and high yield.

The detailed microstructure information of BNNS-t was further exhibited by SEM and TEM. As shown in Figure 3a, the BNNS-t sheets are substantially thinner, all within tens of nanometers, than the 100 nm reference thickness given in the SEM image. The TEM image of BNNS-t in Figure 3b demonstrates that BNNS-t is a stack of numerous smaller BNNS, which further indicates that BNNS-t is prone to breaking to form angular-shaped nanosheets. Figure 3c displays the TEM image of BNNS-t at high magnification, indicating its ultrathin characteristic, which is consistent with the result obtained by the SEM image. The lattice fringe spacing is 0.25 nm for BNNS-t, as shown in Figure 3d, and it is a good match for the (100) plane of hexagonal boron nitride.

The chemical structural information of BNNS was effectively characterized by the Reflex Raman system and FT-IR. As shown in Figure 4a, the Raman peaks of BNNS-t and BNNS-b are located at 1365.9 and 1363.4 cm^{-1}, respectively. Both peaks display the BN structure and are related to the E_{2g} phonon mode of BN.[37] The infrared spectra of BNNS-t and BNNS-b are shown in Figure 4b. Two characteristic absorption peaks of BNNS-t are located at 1373.58 and 820.70 cm^{-1}, respectively. The characteristic peak at 1373.58 cm^{-1} can be ascribed to the B−N stretching, and the characteristic peak at 820.70 cm^{-1} owes to the B−N−B bending.[38,39] Regarding the reference BNNS-b, two distinctive absorption peaks are observed at 1373.71 and 819.05 cm^{-1}, and an additional peak is observed at 3449.66 cm^{-1}, which may have been

https://doi.org/10.1021/acsomega.2c06013
ACS Omega 2022, 7, 43273−43282

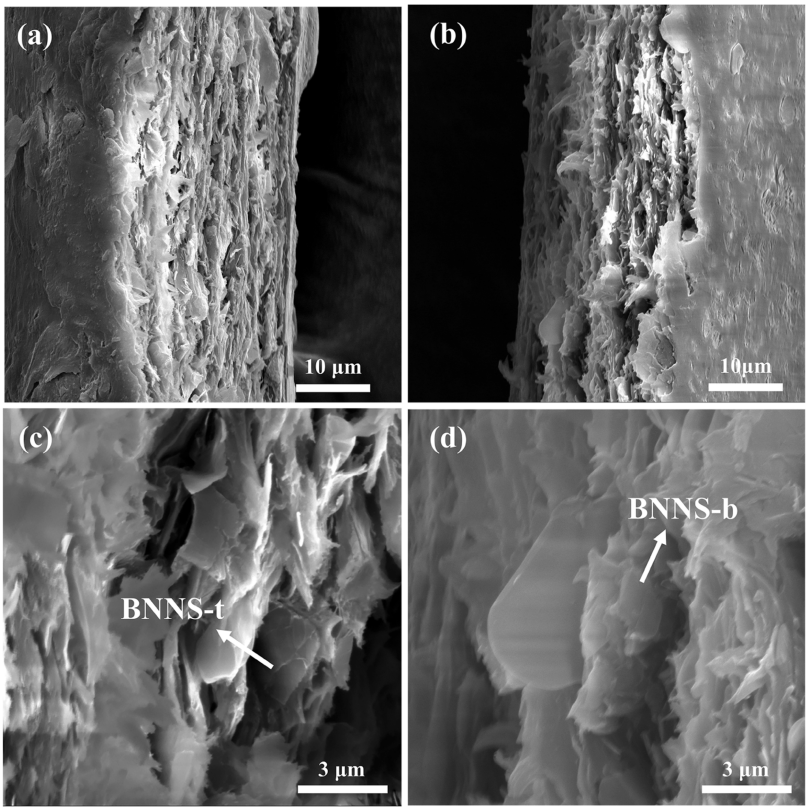

Figure 5. Cross-sectional SEM images of (a, c) 40-PI/BNNS-t and (b, d) 40-PI/BNNS-b.

brought on by the adhesion of water molecules to the surface of the BNNS-b or the hydroxyl group at the border of the BNNS-b.[40] In addition, no impurity peaks that might affect the thermal conductivity of BNNS-t are found in the infrared spectrum. Hence, there are no additional functional groups in the as-obtained BNNS-t by the NaCl template method, which allows the resulting BNNS-t to retain its inherent high thermal conductivity.[41]

The crystal structure of the product was efficiently investigated by XRD. As shown in Figure 4c, the four strong diffraction peaks of BNNS-t are consistent with the diffraction peaks corresponding to the (002), (100), (101), and (004) planes of h-BN (JCPDS card 34-0421). Additionally, the characteristic peaks of impurities are not detected within the detection limit of X-ray diffraction, indicating that pure BNNS can be obtained using the NaCl template method. The results show that the full width at half maximum of the diffraction peak of BNNS-t (002) is 0.663°, much larger than that of BNNS-b (0.272°). In general, the nucleated boron nitride grains grow along the *c*-axis. That is, the thickness direction of boron nitride nanosheets is the c-axis direction. Therefore, the full width at half maximum of the (002) diffraction peak corresponding to the *c*-axis is related to the thickness of the boron nitride nanosheets. In addition, the diffraction peak width in the c-axis direction of BNNS-b prepared by the ball milling method results from the interplay between the microstrain and thickness reduction caused by mechanical friction. Hence, it is reasonable to believe that the thinner thickness BNNS-t can be prepared by the NaCl template method. As a result, based on the SEM and XRD patterns of the above-mentioned two boron nitride nanosheets, BNNS-t has a higher aspect ratio, which is advantageous for heat conduction.[22]

The elemental composition of BNNS was effectively demonstrated by XPS. As shown in Figure 4d, the XPS spectra of BNNS-t and BNNS-b are similar. There is no impurity in the XPS spectra, suggesting that no other contaminants were added during the fabrication. It is advantageous to improve the thermal conductivity of boron nitride. As illustrated in Figure 4e,f, the as-obtained binding energies of B 1s and N 1s are observed at 190.6 and 398.2 eV, respectively, which are reasonably consistent with the figures previously published.[42−44] Therefore, there is a hexagonal phase that exists in the obtained BNNS-t. In addition, the relative ratio of boron to nitrogen (B/N) is estimated using the area ratio and sensitivity factor of the B 1s peak and N 1s peak. The result shows that the B/N is about 1.02:1, and it conforms to the stoichiometric property of BN.

3.2. Characterization of PI/BNNS Composite Films.

The cross-sectional SEM images of 40-PI/BNNS-t and 40-PI/BNNS-b are shown in Figure 5a,b. In the PI matrix, both BNNS-t and BNNS-b are uniformly stacked layer by layer, indicating that BNNS-t and BNNS-b are well dispersed without agglomeration. Meanwhile, as shown in Figure 5c,d, BNNS-t is more randomly distributed in the PI matrix instead of the tile distribution of BNNS-b. It can be attributed to the large diameter of BNNS-t and the existence of an angular shape. In addition, both BNNS-t and BNNS-b in the composite films are utterly preserved, demonstrating that short-time and low-power ultrasound only play a dispersive role and do not destroy the sheet structure.

As shown in Figure 6, the in-plane orientation degree of BNNS in the PI matrix can be predicted by measuring the XRD pattern of the PI/BNNS composite films. The orientation degree of BNNS is expressed as the intensity ratio of the diffraction peaks corresponding to the (002) and

https://doi.org/10.1021/acsomega.2c06013
ACS Omega 2022, 7, 43273−43282

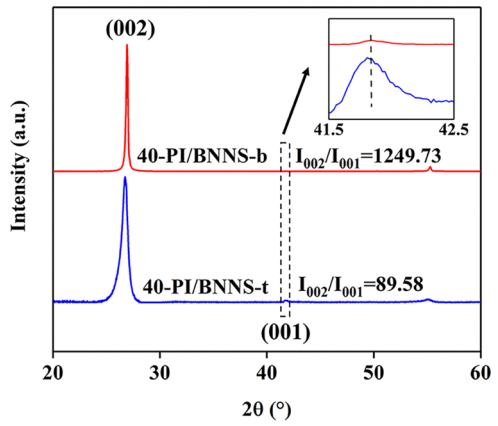

Figure 6. XRD patterns of 40-PI/BNNS-b and 40-PI/BNNS-t.

(100) planes (I_{002} /I_{100}). The ratio of I_{002}/I_{100} (40-PI/BNNS-t) is 89.58, which is much smaller than that of 40-PI/BNNS-b (1249.73). In other words, compared with BNNS-b, the distribution of BNNS-t in the PI matrix is more random. The above result corresponds to the conclusions of the SEM images.

To characterize the thermal properties of PI/BNNS, the composite films were prepared by doping different loading of BNNS into the PI matrix. The out-of-plane thermal diffusivity and the out-of-plane thermal conductivity of the composite films with varying loading of BNNS are shown in Figure 7a,b, respectively. Obviously, with the increasing mass fraction of the filler, the composite films' out-of-plane thermal diffusivity and out-of-plane thermal conductivity will increase accordingly. When the filling loading is 10%, the thermal conductivities of PI/BNNS-t and PI/BNNS-b are both 0.42 W m^{-1} K^{-1}. However, when the filling loading of fillers is increased, the out-of-plane thermal conductivity of PI/BNNS-t is higher than that of PI/BNNS-b, and the gap in the thermal conductivity between PI/BNNS-t and PI/BNNS-b is enlarged. The differential in thermal conductivity develops progressively with the increase in filler mass fraction. When the filling loading is 40%, the out-of-plane thermal conductivity of PI/BNNS-t is 0.09 W m^{-1} K^{-1} higher than that of PI/BNNS-b, which is attributed to the existence of an angular shape and the large aspect ratio of BNNS-t. At low filling levels, fillers are separated from fillers by the PI matrix and do not touch each other, rendering the curved edges ineffective. At high filling levels, the curved edges of BNNS-t will play an auxiliary role in the out-of-plane thermal conduction, providing a connection to facilitate the construction of thermal conduction paths. Additionally, the larger aspect ratio of BNNS-t makes it easier to bend than BNNS-b, which is more conducive to establishing a 3D thermal conductive network. The results show that the angular shape and high aspect ratio of PI/BNNS-t can obtain better out-of-plane thermal properties.

The out-of-plane thermal conductivity of the composite films was further characterized by infrared imaging. First, an LED light sticker (3 W) was set up on the table, the power was turned on, and then after 5 min, the temperature of the LED light sticker was stabilized. After that, the film was placed on the LED light sticker, and an infrared camera was used to record the curve of the highest temperature point on the film over time. The composite films used for the out-of-plane thermal conductivity measurement are shown in Figure 8a, in which the out-of-plane thermal conductivities of PI, 40-PI/BNNS-b, and 40-PI/BNNS-t are 0.19, 0.58, and 0.67 W m^{-1} K^{-1}, respectively. In addition, Figure 8b,c displays the curves and infrared images of the highest temperature point on the surface of PI, 40-PI/BNNS-b, and 40-PI/BNNS-t, respectively. In the front part of the three curves, it can be seen that the heating rates of 40-PI/BNNS-t, 40-PI/BNNS-b, and PI decrease successively, which indicates that of the three kinds of films, the best out-of-plane thermal conduction property of 40-PI/BNNS-t is obtained. Furthermore, the highest surface temperature of PI is stable at about 143 °C, the highest surface temperature of 40-PI/BNNS-b is steady at about 156 °C, and 40-PI/BNNS-t is stable at about 176 °C. The data above are consistent with the findings of the out-of-plane thermal conductivities, and they can also reflect the differences in thermal conductivities of the three different types of films. As a result, the as-prepared BNNS-t by the NaCl template method has a significant impact on the thermal properties of the composite films.

4. CONCLUSIONS

In summary, to improve the out-of-plane thermal conductivity of the composite films, the angular-shaped boron nitride nanosheet with a high aspect ratio, namely a network structure element with uniform thermal conductivity, was prepared and applied to the PI/BNNS composite films. The method for synthesizing the high aspect ratio and the stable and uniform lateral dimension of 2D BNNS was developed using recrystal-

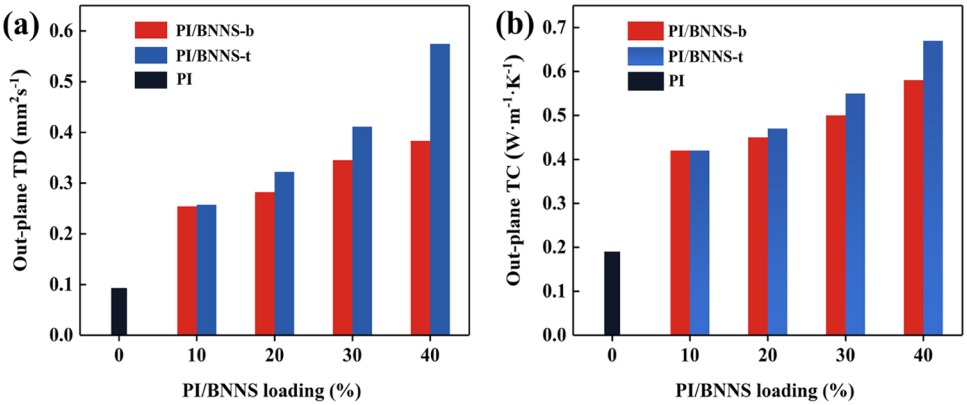

Figure 7. (a) Out-of-plane thermal diffusivities (TD) and (b) conductivities (TC) of the composite films as a function of the loading of BNNS-t and BNNS-b.

https://doi.org/10.1021/acsomega.2c06013
ACS Omega 2022, 7, 43273−43282

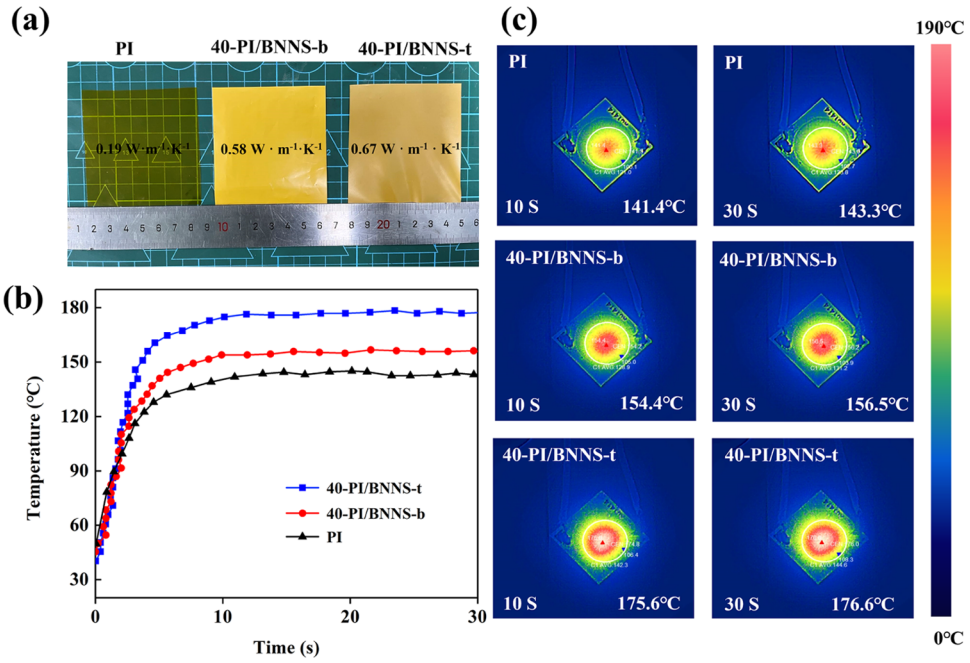

Figure 8. (a) Photographs of PI, 40-PI/BNNS-b, and 40-PI/BNNS-t, (b) the highest temperature of the composite films varies with the running time of the LED used, and (c) the corresponding IR images.

lized NaCl as the template. The as-obtained BNNS are mainly large-area flakes with an average lateral size of 3 μm and a total yield of as high as 77%. Meanwhile, the addition of BNNS-t with a high aspect ratio and a unique angular-shaped structure can significantly improve the out-of-plane thermal properties of the PI composite film, and the out-of-plane thermal conductivity of the composite film can achieve 0.67 W m^{-1} K^{-1} when the filling loading is 40%. In addition, BNNS prepared by the template method can provide a new idea for the research of the thermal properties of composite materials.

AUTHOR INFORMATION

Corresponding Authors

Xiaomin Li − *Institute of Photovoltaics, Nanchang University, Nanchang 330031, China*; orcid.org/0000-0002-1228-1677; Phone: 0791-83969329; Email: lixiaomin@ncu.edu.cn

Chuanqiang Yin − *Institute of Photovoltaics, Nanchang University, Nanchang 330031, China*; Email: cqyin@ncu.edu.cn

Authors

Song Zuo − *Institute of Photovoltaics, Nanchang University, Nanchang 330031, China*

Yu Lan − *Institute of Photovoltaics, Nanchang University, Nanchang 330031, China*

Jinpeng Luo − *Institute of Photovoltaics, Nanchang University, Nanchang 330031, China*

Fei Zhou − *Institute of Photovoltaics, Nanchang University, Nanchang 330031, China*

Lexiang Xu − *Institute of Photovoltaics, Nanchang University, Nanchang 330031, China*

Shaoxiong Xie − *Institute of Photovoltaics, Nanchang University, Nanchang 330031, China*

Xiuqin Wei − *Institute of Photovoltaics, Nanchang University, Nanchang 330031, China*

Lang Zhou − *Institute of Photovoltaics, Nanchang University, Nanchang 330031, China*

Lei Ma − *Guangxi Key Laboratory of Information Materials, Guilin University of Electronic Technology, Guilin 541004, China*

Complete contact information is available at: https://pubs.acs.org/10.1021/acsomega.2c06013

Author Contributions

The manuscript was written through contributions of all authors. All authors have given approval to the final version of the manuscript.

Notes

The authors declare no competing financial interest.

ACKNOWLEDGMENTS

This work was financially supported by the Youth Long-term Project of Jiangxi Province to Introduce Leading Innovative Talents, China (Grant No. jxsq2018106023), The Guangxi Key Laboratory of Information Materials (211012-K), and Postgraduate Innovation Special Fund Project of Jiangxi Province, China (Grant No. YC2021-S121).

ABBREVIATIONS

PI/BNNS, polyimide/boron nitride nanosheet; BNNS, boron nitride nanosheet; LED, light-emitting diodes; h-BN, hexagonal boron nitride; DMAc, *N*,*N*-dimethylacetamide; PMDA, pyromellitic dianhydride; ODA, 4,4′-oxydianiline; PAA, polyimide acid

REFERENCES

(1) Yang, G.; Wang, M.; Dong, J.; Su, F.; Ji, Y.; Liu, C.; Shen, C. Fibers-induced segregated-like structure for polymer composites achieving excellent thermal conductivity and electromagnetic interference shielding efficiency. *Composites, Part B* **2022**, *246*, No. 110253.

(2) Wu, Z.; Xu, C.; Ma, C.; Liu, Z.; Cheng, H. M.; Ren, W. Synergistic effect of aligned graphene nanosheets in graphene foam for high-performance thermally conductive composites. *Adv. Mater.* **2019**, *31*, No. 1900199.
(3) Ma, M.; Xu, L.; Qiao, L.; Chen, S.; Shi, Y.; He, H.; Wang, X. Nanofibrillated Cellulose/MgO@rGO composite films with highly anisotropic thermal conductivity and electrical insulation. *Chem. Eng. J.* **2020**, *392*, No. 123714.
(4) Zhang, C.; Huang, R.; Wang, Y.; Wu, Z.; Zhang, H.; Li, Y.; Wang, W.; Huang, C.; Li, L. Self-assembled boron nitride nanotube reinforced graphene oxide aerogels for dielectric nanocomposites with high thermal management capability. *ACS Appl. Mater. Interfaces* **2020**, *12*, 1436−1443.
(5) Choi, K.; Lee, J.; Choi, H.; Kim, G.-W.; Kim, H. I.; Park, T. Heat dissipation effects on the stability of planar perovskite solar cells. *Energy Environ. Sci.* **2020**, *13*, 5059−5067.
(6) Zhang, Y.; Hao, N.; Lin, X.; Nie, S. Emerging challenges in the thermal management of cellulose nanofibril-based supercapacitors, lithium-ion batteries and solar cells: A review. *Carbohydr. Polym.* **2020**, *234*, No. 115888.
(7) Li, M. D.; Shen, X. Q.; Chen, X.; Gan, J. M.; Wang, F.; Li, J.; Wang, X. L.; Shen, Q. D. Thermal management of chips by a device prototype using synergistic effects of 3-D heat-conductive network and electrocaloric refrigeration. *Nat. Commun.* **2022**, *13*, No. 5849.
(8) Evans, A. M.; Giri, A.; Sangwan, V. K.; Xun, S.; Bartnof, M.; Torres-Castanedo, C. G.; Balch, H. B.; Rahn, M. S.; Bradshaw, N. P.; Vitaku, E.; et al. Thermally conductive ultra-low-k dielectric layers based on two-dimensional covalent organic frameworks. *Nat. Mater.* **2021**, *20*, 1142−1148.
(9) Kang, S. J.; Hong, H.; Jeong, C.; Lee, J. S.; Ryu, H.; Yang, J.-h.; Kim, J. U.; Shin, Y. J.; Kim, T.-i. Avoiding heating interference and guided thermal conduction in stretchable devices using thermal conductive composite islands. *Nano Res.* **2021**, *14*, 3253−3259.
(10) Duan, G.; Cao, Y.; Quan, J.; Hu, Z.; Wang, Y.; Yu, J.; Zhu, J. Bioinspired construction of BN@polydopamine@Al_2O_3 fillers for preparation of a polyimide dielectric composite with enhanced thermal conductivity and breakdown strength. *J. Mater. Sci.* **2020**, *55*, 8170−8184.
(11) Guo, Y.; Ruan, K.; Shi, X.; Yang, X.; Gu, J. Factors affecting thermal conductivities of the polymers and polymer composites: A review. *Compos. Sci. Technol.* **2020**, *193*, No. 108134.
(12) Cai, Q.; Scullion, D.; Gan, W.; Falin, A.; Zhang, S.; Watanabe, K.; Taniguchi, T.; Chen, Y.; Santos, E. J. G.; Li, L. H. High thermal conductivity of high-quality monolayer boron nitride and its thermal expansion. *Sci. Adv.* **2019**, *5*, No. eaav0129.
(13) An, L.; Gu, R.; Zhong, B.; Wang, J.; Zhang, J.; Yu, Y. Quasi-Isotropically Thermal conductive, highly transparent, insulating and super-flexible polymer films achieved by cross linked 2D hexagonal boron nitride nanosheets. *Small* **2021**, *17*, No. 2101409.
(14) An, L.; Zhang, N.; Zeng, X.; Zhong, B.; Yu, Y. Quasi-isotropically thermoconductive, antiwear and insulating hierarchically assembled hexagonal boron nitride nanosheet/epoxy composites for efficient microelectronic cooling. *J. Colloid Interface Sci.* **2022**, *608*, 1907−1918.
(15) Pacilé, D.; Meyer, J. C.; Girit, Ç. Ö.; Zettl, A. The two-dimensional phase of boron nitride: Few-atomic-layer sheets and suspended membranes. *Appl. Phys. Lett.* **2008**, *92*, 223−225.
(16) Li, L. H.; Chen, Y.; Behan, G.; Zhang, H.; Petravic, M.; Glushenkov, A. M. Large-scale mechanical peeling of boron nitride nanosheets by low-energy ball milling. *J. Mater. Chem.* **2011**, *21*, 11862−11866.
(17) Lee, D.; Lee, B.; Park, K. H.; Ryu, H. J.; Jeon, S.; Hong, S. H. Scalable exfoliation process for highly soluble boron nitride nanoplatelets by hydroxide-assisted ball milling. *Nano Lett.* **2015**, *15*, 1238−1244.
(18) Wu, G.; Yi, M.; Xiao, G.; Chen, Z.; Zhang, J.; Xu, C. A novel method for producing boron nitride nanosheets via synergistic exfoliation with pure shear ball milling and ultrasonication. *Ceram. Int.* **2019**, *45*, 23841−23848.
(19) Zhou, Y.; Xu, L.; Liu, M.; Qi, Z.; Wang, W.; Zhu, J.; Chen, S.; Yu, K.; Su, Y.; Ding, B.; et al. Viscous solvent-assisted planetary ball milling for the scalable production of large ultrathin two-dimensional materials. *ACS Nano* **2022**, *16*, 10179−10187.
(20) Tian, R.; Jia, X.; Lan, M.; Yang, J.; Wang, S.; Li, Y.; Shao, D.; Feng, L.; Song, H. Efficient exfoliation and functionalization of hexagonal boron nitride using recyclable ionic liquid crystal for thermal management applications. *Chem. Eng. J.* **2022**, *446*, No. 137255.
(21) Li, M.; Wang, M.; Hou, X.; Zhan, Z.; Wang, H.; Fu, H.; Lin, C.-T.; Fu, L.; Jiang, N.; Yu, J. Highly thermal conductive and electrical insulating polymer composites with boron nitride. *Composites, Part B* **2020**, *184*, No. 107746.
(22) Yan, Q.; Dai, W.; Gao, J.; Tan, X.; Lv, L.; Ying, J.; Lu, X.; Lu, J.; Yao, Y.; Wei, Q.; et al. Ultrahigh-aspect-ratio boron nitride nanosheets leading to superhigh in-plane thermal conductivity of foldable heat spreader. *ACS Nano* **2021**, *15*, 6489−6498.
(23) Lei, W.; Mochalin, V. N.; Liu, D.; Qin, S.; Gogotsi, Y.; Chen, Y. Boron nitride colloidal solutions, ultralight aerogels and freestanding membranes through one-step exfoliation and functionalization. *Nat. Commun.* **2015**, *6*, No. 8849.
(24) Morishita, T.; Okamoto, H.; Katagiri, Y.; Matsushita, M.; Fukumori, K. A high-yield ionic liquid-promoted synthesis of boron nitride nanosheets by direct exfoliation. *Chem. Commun.* **2015**, *51*, 12068−12071.
(25) Yuan, F.; Jiao, W.; Yang, F.; Liu, W.; Liu, J.; Xu, Z.; Wang, R. Scalable exfoliation for large-size boron nitride nanosheets by low temperature thermal expansion-assisted ultrasonic exfoliation. *J. Mater. Chem. C* **2017**, *5*, 6359−6368.
(26) Yu, B.; Fan, J.; He, J.; Liu, Y.; Wang, R.; Qi, K.; Han, P.; Luo, Z.Boron nitride nanosheets: large-scale exfoliation in NaOH-LiCl solution and their highly thermoconductive insulating nanocomposite paper with PI via electrospinning-electrospraying. *J. Alloys Compd.930*, 167303. DOI: 10.1016/j.jallcom.2022.167303.
(27) Zhang, C.; Wang, M.; Lin, X.; Tao, S.; Wang, X.; Chen, Y.; Liu, H.; Wang, Y.; Qi, H. Holocellulose nanofibrils assisted exfoliation of boron nitride nanosheets for thermal management nanocomposite films. *Carbohydr. Polym.* **2022**, *291*, No. 119578.
(28) Kim, S. M.; Hsu, A.; Park, M. H.; Chae, S. H.; Yun, S. J.; Lee, J. S.; Cho, D. H.; Fang, W.; Lee, C.; Palacios, T.; et al. Synthesis of large-area multilayer hexagonal boron nitride for high material performance. *Nat. Commun.* **2015**, *6*, No. 8662.
(29) Caneva, S.; Weatherup, R. S.; Bayer, B. C.; Blume, R.; Cabrero-Vilatela, A.; Braeuninger-Weimer, P.; Martin, M. B.; Wang, R.; Baehtz, C.; Schloegl, R.; et al. Controlling catalyst bulk reservoir effects for monolayer hexagonal boron nitride CVD. *Nano Lett.* **2016**, *16*, 1250−1261.
(30) Ruckhofer, A.; Sacchi, M.; Payne, A.; Jardine, A. P.; Ernst, W. E.; Avidor, N.; Tamtögl, A. Evolution of ordered nanoporous phases during h-BN growth: Controlling the route from gas-phase precursor to 2D material by in-situ monitoring. *Nanoscale Horiz.* **2022**, *7*, 1388−1396.
(31) Gao, R.; Yin, L.; Wang, C.; Qi, Y.; Lun, N.; Zhang, L.; Liu, Y.-X.; Kang, L.; Wang, X. High-yield synthesis of boron nitride nanosheets with strong ultraviolet cathodoluminescence emission. *J. Phys. Chem. C* **2009**, *113*, 15160−15165.
(32) Wang, X.; Zhi, C.; Li, L.; Zeng, H.; Li, C.; Mitome, M.; Golberg, D.; Bando, Y. "Chemical blowing" of thin-walled bubbles: high-throughput fabrication of large-area, few-layered BN and C(x)-BN nanosheets. *Adv. Mater.* **2011**, *23*, 4072−4076.
(33) Pan, D.; Dong, J.; Yang, G.; Su, F.; Chang, B.; Liu, C.; Zhu, Y.-C.; Guo, Z. Ice template method assists in obtaining carbonized cellulose/boron nitride aerogel with 3D spatial network structure to enhance the thermal conductivity and flame retardancy of epoxy-based composites. *Adv. Compos. Hybrid Mater.* **2022**, *5*, 58−70.
(34) Yang, W.; Wang, Y.; Li, Y.; Gao, C.; Tian, X.; Wu, N.; Geng, Z.; Che, S.; Yang, F.; Li, Y. Three-dimensional skeleton assembled by carbon nanotubes/boron nitride as filler in epoxy for thermal

management materials with high thermal conductivity and electrical insulation. *Composites, Part B* **2021**, *224*, No. 109168.
(35) Guiney, L. M.; Mansukhani, N. D.; Jakus, A. E.; Wallace, S. G.; Shah, R. N.; Hersam, M. C. Three-Dimensional printing of cytocompatible, thermally conductive hexagonal boron nitride nanocomposites. *Nano Lett.* **2018**, *18*, 3488−3493.
(36) Xu, Y.; Li, T.; Xu, W.; Li, C.; E, S.; Wang, L.; Long, X.; Bai, Y.; Xu, L.; Yao, Y. Scalable production of high-quality boron nitride nanosheets via a recyclable salt-templating method. *Green Chem.* **2019**, *21*, 6746−6753.
(37) Wu, N.; Yang, W.; Li, H.; Che, S.; Gao, C.; Jiang, B.; Li, Z.; Xu, C.; Wang, X.; Li, Y. Amino acid functionalized boron nitride nanosheets towards enhanced thermal and mechanical performance of epoxy composite. *J. Colloid Interface Sci.* **2022**, *619*, 388−398.
(38) Shi, Y.; Hamsen, C.; Jia, X.; Kim, K. K.; Reina, A.; Hofmann, M.; Hsu, A. L.; Zhang, K.; Li, H.; Juang, Z. Y.; et al. Synthesis of few-layer hexagonal boron nitride thin film by chemical vapor deposition. *Nano Lett.* **2010**, *10*, 4134−4139.
(39) Nazarov, A. S.; Demin, V. N.; Grayfer, E. D.; Bulavchenko, A. I.; Arymbaeva, A. T.; Shin, H. J.; Choi, J. Y.; Fedorov, V. E. Functionalization and dispersion of hexagonal boron nitride (h-BN) nanosheets treated with inorganic reagents. *Chem. - Asian J.* **2012**, *7*, 554−560.
(40) Weng, Q.; Kvashnin, D. G.; Wang, X.; Cretu, O.; Yang, Y.; Zhou, M.; Zhang, C.; Tang, D. M.; Sorokin, P. B.; Bando, Y.; Golberg, D. Tuning of the optical, electronic, and magnetic properties of boron nitride nanosheets with oxygen doping and functionalization. *Adv. Mater.* **2017**, *29*, No. 1700695.
(41) Burger, N.; Laachachi, A.; Ferriol, M.; Lutz, M.; Toniazzo, V.; Ruch, D. Review of thermal conductivity in composites: Mechanisms, parameters and theory. *Prog. Polym. Sci.* **2016**, *61*, 1−28.
(42) An, L.; Yang, Z.; Zeng, X.; Hu, W.; Yu, Y.; Zhang, J.; Wang, Q. Flexible and quasi-isotropically thermoconductive polyimide films by guided assembly of boron nitride nanoplate/boron nitride flakes for microelectronic application. *Chem. Eng. J.* **2022**, *431*, No. 133740.
(43) Li, Y.; Huang, T.; Chen, M.; Wu, L. Simultaneous exfoliation and functionalization of large-sized boron nitride nanosheets for enhanced thermal conductivity of polymer composite film. *Chem. Eng. J.* **2022**, *442*, No. 136237.
(44) Jiang, H.; Cai, Q.; Mateti, S.; Yu, Y.; Zhi, C.; Chen, Y. Boron nitride nanosheet dispersion at high concentrations. *ACS Appl. Mater. Interfaces* **2021**, *13*, 44751−44759.

https://doi.org/10.1021/acsomega.2c06013
ACS Omega 2022, 7, 43273−43282